

Low Frequency Radio Observations Of W51 Complex

A.Pramesh Rao,¹ P.K. Srivastava ²

¹ NCRA, TIFR, Pune, India 411007 *

² DAV College, Kanpur, India 208001

Accepted???.Received????;in original form ????

ABSTRACT

W51 is a giant radio complex lying along the tangent to the Sagittarius arm at a distance of about 7kpc from Sun, with an extension of about 1° in the sky. It is divided into three components A,B,C where W51A and W51B are regions consisting of many compact HII sources. We have made continuum radio observations of these HII regions of W51 complex at 240,610,1060,1400 MHz frequencies using GMRT. The observed spectrum for each of the prominent subcomponents of W51A, G49.5-0.4 and G49.4-0.3 has been obtained by least-square fitting of flux and frequency to free-free emission spectrum and physical properties like electron temperature and emission measure have been derived from it for each of the discrete sources. Electron temperatures, estimated from continuum spectrum, are found to be low and different from the temperatures reported from RRL studies of these HII regions. We propose a simple two component model to account for the apparent discrepancy between RRL temperature and electron temperature obtained from fit including higher frequencies as well.

Key words: ISM:HII regions:radio continuum:individual(W51)

1 INTRODUCTION

W51 is a giant radio complex, lying along the tangent to the Sagittarius arm at a distance of about 7kpc and extending to about 1° in the field of view. The entire complex consists of many HII regions of varying morphologies and compactness, embedded into an extended and diffused nebulous emission. According to convention adopted by Kundu & Velusamy(1967) all the compact HII regions in the complex are divided into two components W51A and W51B; the third component W51C is supposed to be a SNR (Copetti & Schmidt 1991). The entire complex is optically obscure. It has been observed in radio frequencies extensively and the early observations were reviewed by Bieging(1975). The brightest HII sources are found in W51A, which itself consists of two subcomponents G49.5-0.4 and G49.4-0.3. G49.5-0.4 is the most luminous star forming region in the entire complex and has been studied in details. High resolution radio continuum observations (Martin 1972; Mehringer 1994; Subrahmanyan & Goss 1995) have observed atleast 8 prominent compact sources in G49.5-0.4; these are referred to as G49.5-0.4 *a,b,...,h* in order of increasing right ascension; similarly G49.4-0.3 consists of atleast 3 compact sources G49.4-0.3 *a,b,c* (Martin 1972). Mehringer has reported many

more sources in G49.5-0.4 from 20cm observations at higher resolution of $15'' \times 13''$.

Radio recombination line (RRL) studies of G49.5-0.4 have been done to study the kinematics and local thermodynamic equilibrium(LTE) electron temperature(T_e) of this region. H109 α RRL observations by Wilson et al(1970) with a resolution of 4 arcmin and by Pankonin,Payne and Terzian (1979) at resolution 2.6 arcmin show that $T_e \sim 6000$ K in G49.5-0.4. Lower frequency observations for H137 β and H166 α lines show higher temperatures, 8500K and 7100K (Pankonin et al. 1979) respectively . Since lower frequency lines are expected to arise from outer, lower density parts of the HII regions, the above results indicate that there is a temperature gradient increasing radially outward (Churchwell et al 1978). From observations of H92 α lines Mehringer(1994) concludes that T_e varies from 4700 to 11000K with an average of 7800 ± 1200 K. All the RRL results have been derived under LTE approximation.

Electron temperature is one of the most important parameters to understand the physical properties of thermal HII regions. Low frequency continuum observations offer a direct estimate of electron temperatures due to optical depth effects. Meter-wavelength observations at 151MHz by Copetti & Schmidt(1991) and at 410MHz by Shaver(1969) show that T_e in G49.5-0.4 is 3500 ± 700 K and 4650 ± 500 K respectively. Since low frequency continuum observations are also biased towards outer parts of HII region, the above re-

* pramesh@ncra.tifr.res.in

sults indicate a radial decrease in temperature from the core, which is opposite to trend seen in RRL studies. However, Subrahmanyan & Goss(1995), from 330MHz continuum observation with ~ 1 arcmin resolution, infer a value of at least 7500K towards G49.5-0.4e, the brightest source in G49.5-0.4. It has therefore been argued that low values obtained by Copetti & Schmidt(1991) and Shaver(1969) are due to their poor resolution (> 3 arcmin) images. On the other hand, the effect of pressure broadening at low frequencies in particular and non-LTE effects in general may overestimate the RRL temperatures (Shaver 1980).

In order to determine the electron temperature and other physical parameters in the components W51A and W51B, we have therefore carried out high resolution synthesis continuum imaging of W51 using Giant Meterwave Radio Telescope (GMRT), India, at 240,610,1060, and 1400MHz. This is the first time that W51 has been observed at meter-wavelengths with few arcsec resolutions.

2 OBSERVATIONS AND DATA REDUCTION

2.1 Data Reduction

Full synthesis observations of W51 complex were made with the GMRT during the year 2001. Details of the observational parameters are given in Table 1. All the observations were centred on the component W51A. While the higher frequency maps had smaller fields of view and were restricted to only W51A component, the 240MHz field of view was large enough to cover the entire W51 complex. The observations were made in the standard spectral line mode of GMRT (128 channels, each of 128KHz width). A band pass calibrator, which was also the flux density calibrator (either 3C48 or 3C286 or both), was observed for 15-20 minutes at the beginning or at the end of the observation. The rest of the observation was devoted to W51, with a secondary calibrator observed in between every half an hour or so.

In the offline analysis, which was done using standard AIPS, the data were edited, the antenna bandpass estimated and the spectral channels collapsed to a continuum channel of about 13MHz width. For the 240MHz data, where bandwidth smearing is an issue, the spectral data was averaged to 5 channels of 1.25MHz each. The channel averaged data was then calibrated using the secondary calibrator. At all the frequencies, uniformly weighted maps were made with the full resolution of the GMRT, cleaned, and two rounds of phase self-calibration and one of amplitude were done to make the final map. For the images at 240MHz, wide field corrections were incorporated using the multiple facet imaging option in IMAGR. In order to compare the maps at different frequencies, additional maps were made at the higher frequencies with lower resolution (16 arcsec) comparable with the resolution of the 240MHz map and the 5 and 1.4GHz maps presented by Mehringer(1994). It must be noted that the u - v coverages are different in the different maps which could lead to uncertainties in comparing the maps at different frequencies. A low resolution map (2 arcmin) of the W51 complex was also made at 240MHz to compare with the VLA map at 330MHz (Subrahmanyan & Goss, 1995).

A major limitation of the GMRT during the period of

these observations was that no real time measurement of the system temperature during the observations was available. The change in the system temperature between the primary calibrator and W51 was measured later and the flux densities in the final maps were corrected for this (correction factor ranged from 1.2 to 1.6). All the images were corrected for the primary beam of the GMRT antennas.

2.2 Images and Flux Density

Figure 1 shows full field map of W51 at 240MHz made with a resolution of 2 arcmin in order to compare it with the map obtained by Subrahmanyan & Goss (1995) at 330MHz. We note that the overall features agree very well in the two maps. The thermal sources W51A in the north and W51B in the centre, and the nonthermal source W51C are marked in the figure. The extent of nonthermal emission from the supernova remnant W51C is clearly seen. The shortest spacing in our observations is about 50 wavelengths at 240MHz and given that the angular extent of the source is more than 45 arcmin, we believe that our flux density estimates are seriously affected due to lack of measurements at short spacings. The error in the flux density estimates is about 10 per cent, dominated mainly by systematic uncertainties in calibration.

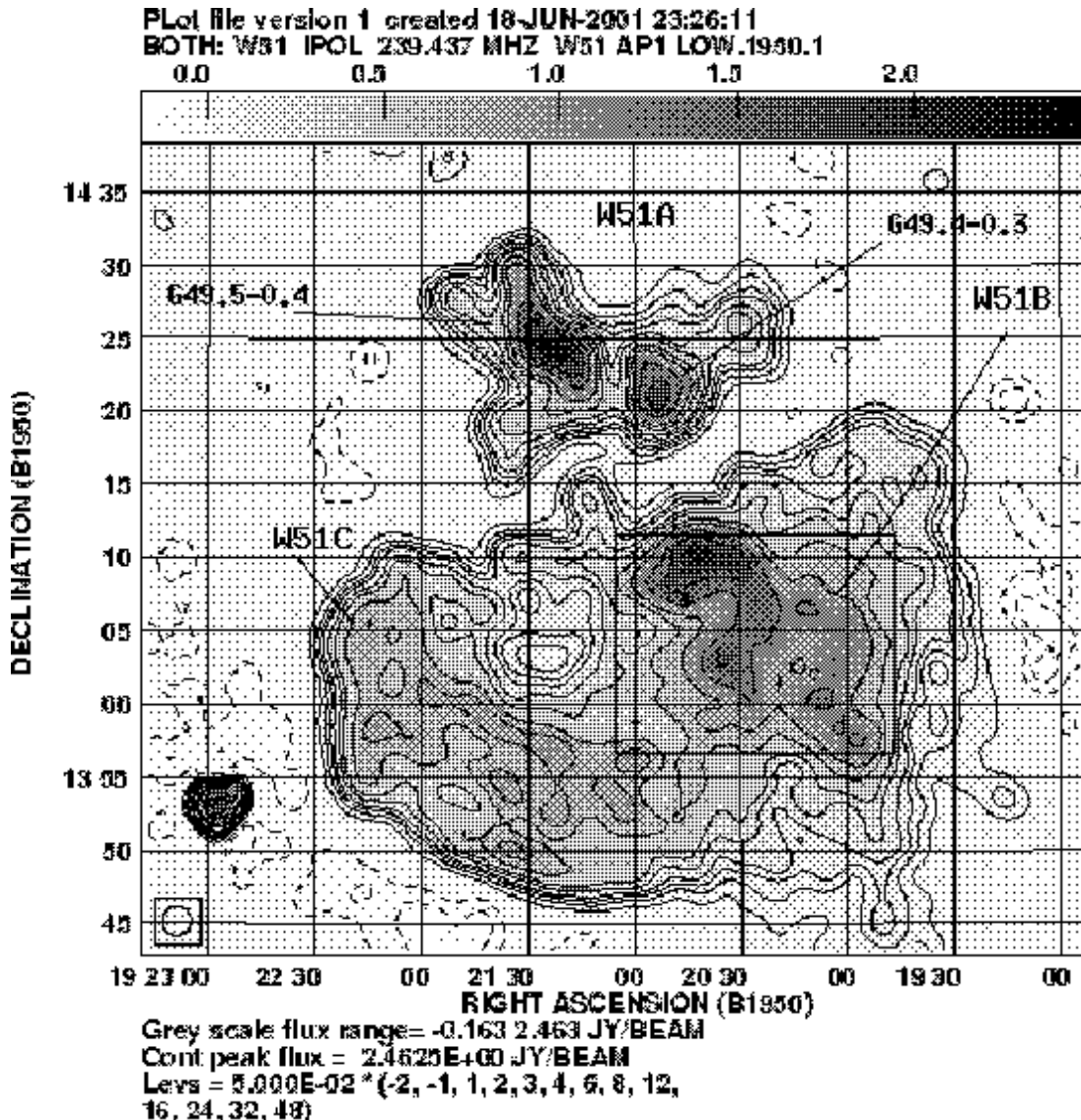
The flux density seen for the W51 complex at 240MHz (Figure 1) is 305 ± 30 Jy, out of which 46 ± 4 Jy lies in W51A. The integrated flux densities in the two subcomponents of W51A, G49.5-0.4 and G49.4-0.3, are 29 ± 3 and 17 ± 2 Jy respectively. These flux densities are consistent with earlier measurements presented in Subrahmanyan & Goss (1995) and with the scenario that these are thermal sources that become optically thick below 1GHz.

The separation of the rest of W51 into W51B and W51C is slightly subjective and if done the way shown in Figure 1, the total flux densities in W51B and W51C are 110 ± 15 and 150 ± 20 Jy respectively. The regions (marked *a*, *b*, *c*, *d*) in W51B corresponding to the sources G49.2-0.4, G49.1-0.4 and G48.9-0.3 (*c*, *d*) respectively, along with the connecting bridge of emission seen at higher frequencies (Subrahmanyan & Goss 1995, Altenhoff et al 1978), are visible in our map too, though all the condensations are fainter than in the 330MHz map of Subrahmanyan & Goss, confirming that they are thermal sources.

The integrated flux density of W51C that we estimate is higher than that estimated by Subrahmanyan & Goss(1995) but this is due to different regions being included in W51C. A more useful quantity is the average surface brightness over W51C at 240MHz with an equivalent circular beam of half power width of 1 arcmin which we estimate to be 0.22 Jy, if we include the entire extent of the source including the fainter extensions to the south west. If we exclude this region, since this may be more appropriate for comparing with the lower dynamic range single dish maps and the 151 MHz maps of Copetti and Schmidt(1991), we find that average surface brightness is 0.29 Jy/beam. These values lie between estimated values at 151 MHz (Copetti & Schmidt 1991) and 330 MHz (Subrahmanyan & Goss 1995) supporting their hypothesis that the brightness temperature of W51C starts to fall below 408 MHz, probably due to internal or foreground free-free absorption. The source 4C13.73 seen outside the south eastern boundary of W51C has a flux density

Table 1. Observational Parameters

Frequency (MHz)	Date	Hours	Bandwidth (MHz)	Resolution (arcsec ²)	Primary calibrator	Secondary calibrator
240	9Mar2001	8	6.25	19x14@50	3C286	1822-096
610	30Aug2001	12	6.25		3C48	1941-154
1057	5Jun2001	8	12.625	17x15@63		
1407	4Jun2001	8	13.25	16x16		

**Figure 1.** Map of full W51 complex at 240MHz with resolution of 2 arcmin

of 4.2 ± 0.3 Jy, and is clearly double in the high resolution maps.

High resolution map of W51A at 240MHz, shown in Figure 2, has a resolution of $20'' \times 15''$ at position angle 45° . Maps with comparable resolution made from the 610,1060 and 1400 MHz observations are also shown in Figure 2. The features seen in our L Band maps agree well with the L Band VLA map published by Mehringer (1994). The regions G49.5-0.4a-h marked by Mehringer are also shown in our map and all of them are thermal sources. These com-

ponents are also seen in the 610MHz map but they become fainter at lower frequencies clearly showing self absorption. In the 240MHz map, detectable emission is present at the location of many of these HII regions though it is not obvious that the emission is from the same physical region as that at higher frequencies. The 240MHz map shows diffuse extended emission not seen in the other maps which is probably due to nonthermal galactic emission which is detected due to the better short spacing coverage at 240MHz. From the images, we have estimated the peak flux density per

beam, normalised to an effective beam area of $1''^2$ for all the sources.

The peak flux density per $1''^2$ beam and the integrated flux of all the HII regions at all the frequencies of observation are presented in Table 2. The integrated flux of the components was estimated by integrating the the flux per beam given in the maps over the region of the component defined by boxes. The definition of boxes defining the region of a component is a bit subjective when it is in a complex region, but we have ensured that all the maps were integrated over identical regions. In Table 2 we have also given the peak flux density for a $1''^2$ beam at 4680 MHz using a map of Mehringer(1994) from the archives of the Astronomical Data Image Library, maintained by the NCSA.

At 240MHz, where the flux density per beam of many of the components is small and the background is high, we have estimated the peak flux of the sources by taking slices across the regions in different directions and estimating the height of the source above the surrounding region. While this was simple for isolated sources, separating the background and the source was often difficult for the sources in complex regions like G49.5-0.4 *c,d,e*. Such a background correction is appropriate when the surrounding flux density comes from regions around or in front of the source. A full justification for or against this procedure requires a detailed understanding of the relative location of all the emitting and absorbing regions which we do not have. However, we feel that this subtraction is justified since there is likely to be foreground emission for the components in complex regions and we were concerned about possible biases in the 240MHz map due to its better short spacing coverage. Making maps at 240MHz with the short spacings removed did not help since the extended emission caused a negative bowl around the extended emission which still needed to be corrected. The estimation of the background and its subtraction produces uncertainties that is reflected in the error bars put on the estimated peak flux density (Fig.4).

A feature of the 240MHz map is the diffused emission to the east and the south east of the W51A complex. This emission is seen in the VLA 330MHz maps, but is not so prominent at the higher frequency maps of both the VLA and the GMRT.

While a more detailed analysis of the higher resolution images at 610MHz and the L Band will be presented elsewhere, we present in Fig.3, a high resolution ($2'' \times 3''$) image of W51A at 1060MHz. The complex nature of the region with the compact sources, shells and diffuse emission, seen in the high resolution images at 5 and 8GHz (Mehringer, 1994), are also seen in our map though with lower peak flux density, with the compact regions showing evidence for self absorption.

3 PHYSICAL CONDITIONS OF W51A COMPONENTS

Both the components in W51A, G49.5-0.4 and G49.4-0.3, consists of several compact HII sources surrounded by diffused ionised gas (Goss & Shaver 1970, Mehringer 1994). The emission from the entire W51A region is regarded as thermal and the sources are seen to be optically thin at frequencies greater than 5GHz (Mar-

tin1972, Mehringer1994). The flux density due to continuum free-free emission from such regions, under the assumption that they form homogeneous isothermal spherical clouds (Hjellming et al 1969), is given by

$$S = 3.07 \times 10^{-2} T_e \nu^2 \Omega (1 - e^{-\tau}) \quad (1)$$

where S is integrated flux density in Jy, T_e is electron temperature in Kelvin, ν is frequency in MHz, Ω is solid angle subtended by the source in steradians and τ is optical depth along the line of sight. At radio wavelengths, optical depth τ is approximately given (Mezger & Henderson 1967) as

$$\tau \sim 1.643 \times 10^5 \nu^{-2.1} EM T_e^{-1.35} \quad (2)$$

where EM is emission measure in cm^{-6}pc . For resolved sources with irregular boundaries, following the procedure adopted by Wood & Churchwell (1989), we consider the value of flux density per synthesized beam at the position of maximum intensity as the best representative of S/Ω . Expressing peak flux density per beam as I (Jy/arcsec 2), Eqs 1 and 2 can be put together as

$$I = a \nu^2 (1 - e^{-b \nu^{-2.1}}) \quad (3)$$

$$\text{where } a = 81.6 \times 10^{-14} T_e, \text{ and } b = 1.643 \times 10^5 EM T_e^{-1.35}$$

We have determined peak flux density per beam I , for a given source, by fitting a gaussian to synthesized beam using JMFIT routine of AIPS; the factor 1.13, arising in the beam area due to gaussian fit has been absorbed in the coefficient a . The integrated flux, for a given source, was determined by using TVSTAT routine of AIPS where care has been taken to use the same blotch area for a given region in different frequency maps. The observed peak intensity I and the integrated flux for each of the sources G49.5-0.4 *a-h* and G49.4-0.3*a-c* are listed in Table 2 for all the four frequencies of observations.

3.1 Electron Temperature

The electron temperature T_e and emission measure EM are then estimated by least-square fitting of the observed data (Table2) into Eq.3. For comparing peak flux density per beam at different frequencies, observed data were normalised by dividing peak flux density per beam by corresponding beam area. The derived values of T_e and EM are given in columns 2 and 3 in Table3. For the purpose of fitting the data, we have also included values of flux density per beam at the higher frequency 4.86GHz observed by Mehringer(1994). The plots of I versus ν for all the sources in G49.5-0.4 and G49.4-0.3 are shown in Figures 4 and 5. The electron temperatures for almost all the HII regions, as obtained from above least-square fitting range between 2100-5600K. The standard model of HII regions is not expected to have such low electron temperatures; the canonical value is generally taken as 10000K.

In fact high resolution interferometric RRL studies of various HII regions in W51A have shown higher electron temperatures. H109 α studies by van Gorkom et al(1980) found T_e for G49.5-0.4 *b,d,e* sources to be 8500,6800,7400K respectively; H76 α studies by Garay et al(1985) found 6600K and 6400K for sources *d,e* respectively; H96 α observations by Mehringer(1994) found average values of T_e around

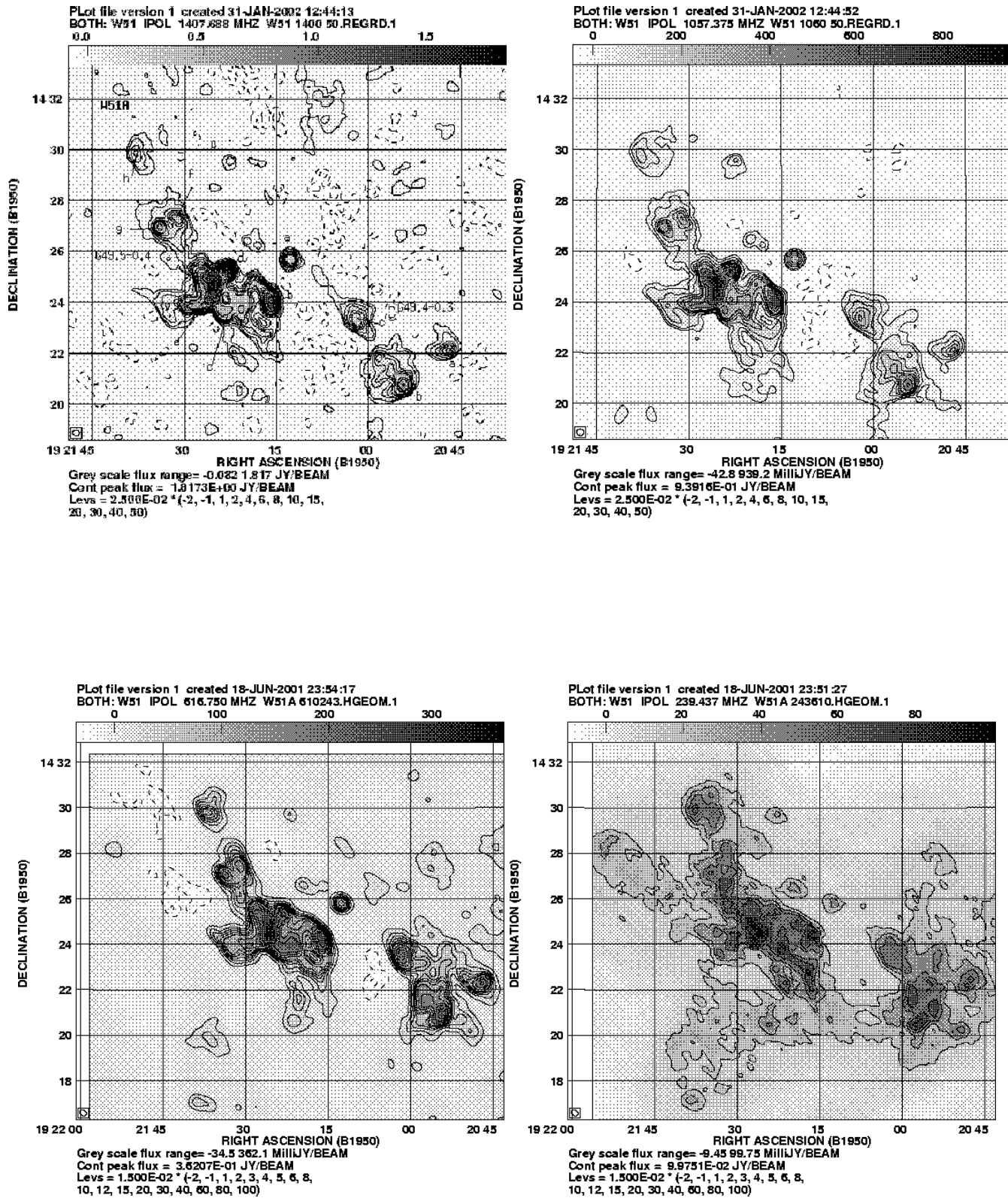


Figure 2. Maps of W51A at 1400,1060,610,240MHz made at appoximately same resolution of $20'' \times 15''$

Table 2. Observed PeakFluxDensity/Beam(mJy/arcsec²)and IntegratedFlux(Jy)

Frequency Beam Size	240MHz (20'' × 15'')		610MHz (20'' × 15'')		1060MHz (16'' × 16'')		1400MHz (15'' × 15'')		4860MHz* (14'' × 13'')
Source	Flux/Beam	Flux	Flux/Beam	Flux	Flux/Beam	Flux	Flux/Beam	Flux	Flux/Beam
G49.5-0.4a	0.22	.273	0.53	.456	1.46	.932	1.97	1.290	1.76
b	0.41	.789	1.09	1.20	4.37	3.62	6.88	5.11	10.15
c	0.41	.622	0.86	.714	2.64	2.04	3.30	1.97	3.76
d	0.12	.423	1.14	.820	4.77	2.81	7.38	3.24	30.11
e	0.30	1.28	1.45	2.37	5.82	7.97	10.13	12.3	35.66
f	0.19	.517	0.59	.624	1.48	1.18	1.61	1.26	2.06
g	0.17	.491	0.68	.546	2.14	1.50	2.46	1.42	3.34
h	0.38	.563	0.40	.410	0.83	.660	0.80	.660	0.90
G49.4-0.3a	0.25		0.76		1.65		2.08		
b	0.28		1.03		3.71		5.42		
c	0.28		0.80		1.68		1.81		

* From Mehringer(1994)

Table 3. Derived Parameters from Least-Square Fitting

Source	T_e (K)	EM (10^6 cm $^{-6}$ pc)	RRL T_e^* (K)
G49.5-0.4a	2300 ± 650	0.5 ± 0.4	$5500-7500$
b	4300 ± 600	3.8 ± 1.8	$5000-6500$
c	3200 ± 550	1.2 ± 0.6	$6000-7500$
d	4300 ± 350	12.3 ± 4.5	$4500-7000$
e	5600 ± 450	15.6 ± 4.8	$6000-8000$
f	2100 ± 200	0.5 ± 0.1	
g	2400 ± 200	0.9 ± 0.2	
h	~ 4900	~ 0.2	
G49.4-0.3a	2750 ± 500	0.5 ± 0.3	
b	3700 ± 350	3.4 ± 3.2	
c	3000 ± 550	0.4 ± 0.25	

brightest components *d,e* in the range of 7500K and 6500K respectively. Similar values of electron temperatures have been reported from other HII regions by RRL studies; e.g. W3A: 7500 ± 750 K (Roelfsema & Goss,1991), SgrA West: 7000 ± 500 K (Roberts & Goss,1993). There is therefore clear discrepancy between electron temperature derived from our least-square fit continuum spectrum and the temperature obtained from RRL studies. We also notice similar discrepancy in the values of emission measures. The best fit values estimated from our continuum observations range between $EM \sim 10^6 - 10^7$ cm $^{-6}$ pc. These values are an order of magnitude less than the values derived in RRL studies(Mehringer 1994).

At sufficiently low frequencies, an HII region is optically thick ($\tau > 1$) so that its continuum brightness temperature becomes equal to electron temperature except for background corrections. The low frequency continuum observations at 151MHz (Copetti & Schmidt 1991) and at 410MHz (Shaver 1969) estimated temperatures of about 3500K and 4650K towards W51A respectively; it has been argued that these low values are perhaps due to their low resolution ($> 3'$) observations. Subrahmanyam & Goss(1995) from their 330MHz continuum observation with 1' resolution inferred that $T_e \sim 7800$ K for G49.5-0.4*d,e* components. We suspect that this is because they (Subrahmanyam & Goss,1995) neglected the immediate background and therefore possibly

over estimated the flux density at 330MHz. We however conclusively find low values of electron temperatures T_e from reasonably good fit between observed flux and frequency (including 610 and 240MHz) to free-free emission spectrum. There is therefore a clear discrepancy between high RRL temperatures and the low values of electron temperatures T_e as given by low frequency observations. Incidentally, though we have taken background correction into account, we also find larger flux density at 240 MHz (and hence correspondingly larger brightness temperature) for some of the sources in W51A as compared to the flux predicted by best fit continuum spectrum; we address to this issue below in Sec.3.2.

Kassim et al(1989) reported similar discrepancy between the flux density observed at 90cm and the estimated flux density at 90cm by fitting the data available at higher frequencies(6cm and 11cm) for the galactic HII regions near S3 complex. They found that their observed flux density at 90cm was lower by an order of magnitude to the estimated value. They assumed the electron temperatures as given by RRL studies and fitted the observed data by reestimating effective sizes of these regions which remained unresolved in their observations. We conjecture that they could have taken lower electron temperatures for the observed regions, without changing the sizes, and obtain similar fit. We suspect that the problem that electron temperatures obtained from thermal spectrum of compact HII regions are lower as compared to that estimated from RRL studies is of generic nature and needs further investigation into the structure and evolution of these regions.

3.2 Two Components Model

Apart from the low value of electron temperature as discussed in previous section, we find that HII regions in W51 fall into two categories: one for which the peak flux density at 240MHz is larger than the value predicted by thermal spectrum (Figs.4 and 5) and the other for which it fits with the spectrum(as in G49.5-0.4 *d,e*).

We notice that all the regions, which show larger observed flux at 240MHz than that predicted by thermal spectrum, are diffused regions with shell type morphology as is evident from 6 and 3cm maps of Mehringer (1994). These re-

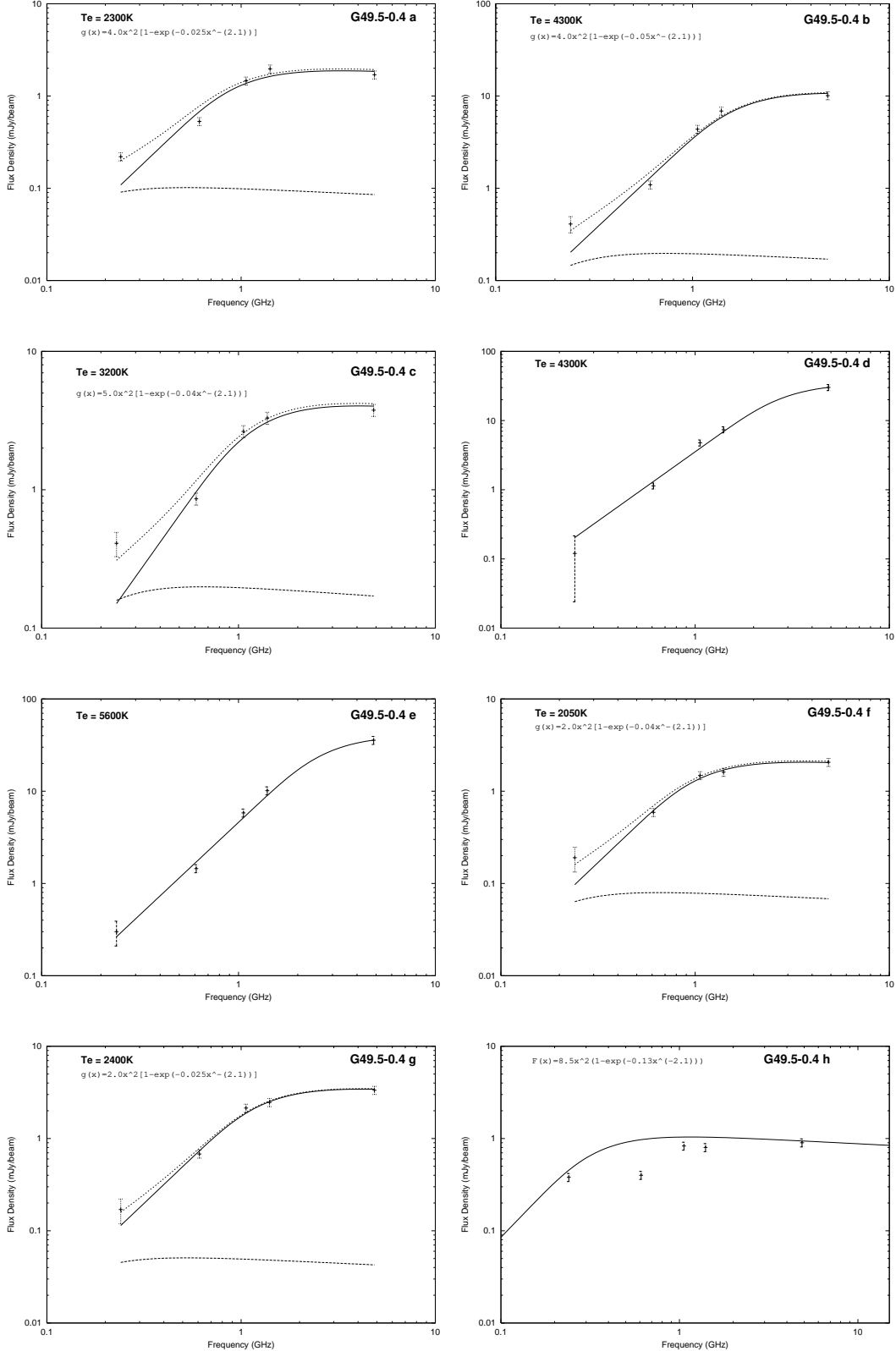


Figure 3. Spectrum of HII regions in G49.5-0.4. Diffused regions *a,b,c,f,g* exhibit two-component structure where solid line shows the spectrum of the core;dashed line shows a possible spectrum of the outer envelope;dotted line shows the resultant which accounts for higher flux at 240MHz. Sources *d,e* are seen to be compact and fit into single component spectrum. Source*h* seems to be optically thin in the entire range

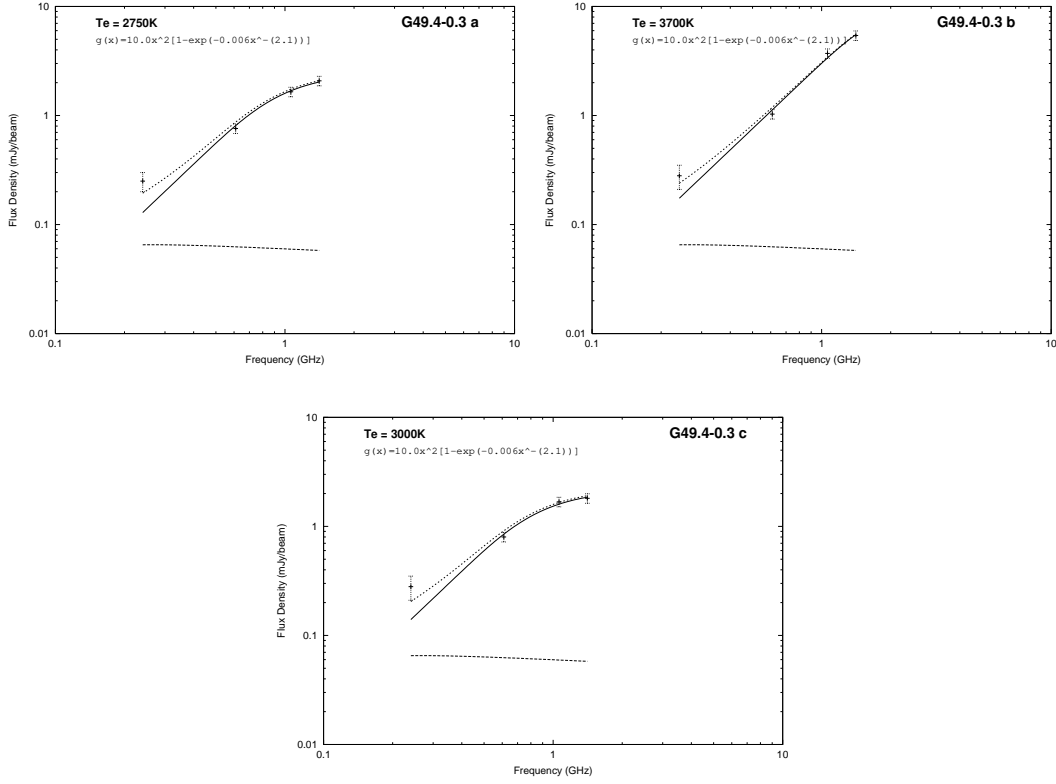


Figure 4. Spectrum of HII compact sources in G49.4-0.3.

gions therefore are likely to have structures. We propose that such HII regions in W51A comprise of two distinct components: component one which consists of dense optically thick core, and another low density hotter ionised optically thin component two which envelopes the core. Most of the flux at high frequencies is observed from component one which shows a turnover at about 1GHz. Low frequency continuum emission from the core and inner parts of the envelope is self-absorbed. The electron temperature in this core region is between 2100-5600K, which is the temperature estimated by us from the fit. The second component, assuming that it is also thermal, is optically thin at all the observed frequencies; it has an almost flat spectrum for $\nu > 240$ MHz and starts turning over at a frequency around 240MHz. The low frequency (240 MHz) continuum emission gets comparable contribution from both the parts (core and envelope) and hence shows corresponding large flux. We emphasize that higher brightness temperature than electron temperature is inconsistent with continuum free-free emission from a single homogeneous source.

We have illustrated the two component model in Figures 3 and 4. Bold line in the plots denote the spectrum obtained from the fit which effectively represents spectrum of inner core. This region shows turnover at about 1GHz and is optically thick at 240MHz. Dashed lines, represented by functions $g(x)$, represent almost flat spectrum of the low density outer envelope which turns over at frequency less than 240MHz. Their superposition shown by dotted curves give the observed resultant spectrum. For example, in case of G49.5-0.4 a, we have assumed that the second outer component has the spectrum

$$I(\nu) = 4.0\nu^2(1 - e^{0.025\nu^{-2.1}})$$

In optically thin regime ($\tau \ll 1$) the flux is related to the product of electron temperature and optical depth (as given by Eq.1),

$$S = 3.07 \times 10^{-2}\nu^2\Omega\tau T_e \quad (4)$$

Therefore from radio continuum data alone we cannot, per se, say anything about electron temperature or emission measure of the outer envelope. However RRL temperatures are estimated to be high (~ 8000 K) in these sources. In order to be consistent with RRL observations, we assume that T_e is large in the envelopes and consequently they are optically thin at the frequencies of observations. In fact RRL studies do not precisely fix the region from which the lines are observed. It is reasonable to assume that RRL lines arise from the high T_e low density ionised envelope, in which case these are likely to be less affected by pressure broadening and are emitted near LTE conditions. It must however be emphasized that our empirical spectrum given by Eq.3 does not uniquely fix but give multiple possible solutions for electron temperature and optical depth of the second component(envelope).

It is possible to account for our observations by assuming a more complicated multi-component model like a raisin pudding model. However we do not see the need for multiple clumps for which there are no signatures observed in any of the high frequency continuum mapping of W51A with higher resolution and sensitivity. We find that a simple two component model is more in conformity with the observations.

Regions G49.5-0.4 d, e where there is good fit found with

observed data, are compact and do not show any structures in high resolution 6 and 3cm maps of Mehringer (1994). The flux density of these sources at 240MHz is not very accurately determined and therefore we have correspondingly used larger error bars. Within error bars, our observed flux and frequency data fits, to the single component thermal spectrum. Lastly, region G49.5-0.4 h defies any reasonable fit to model spectrum (see Fig.3). For this source even the integrated flux density does not seem to change over the entire observed frequency range (Table2). We, therefore, infer that this source is optically thin in the entire range of observation and turns over at frequency less than or equal to 240MHz. As shown in Fig.4, we have drawn a possible spectrum $F(x)$ which puts an upper limit of $T_e < 4900K$ for this region. However there are any number of other solutions possible for the given data set.

4 SUMMARY

We have carried out radio continuum observations of W51 complex at 240, 610, 1060, and 1400MHz frequencies using Giant Meterwave Radio Telescope, India. Observed spectra of prominent HII regions in W51A, G49.5-0.4 and G49.4-0.3, was analysed to derive physical properties like electron temperature and emission measure of these HII regions. The observed spectra confirms that emission is thermal. Fitting the observed flux density and frequency into free-free emission spectrum shows that kinetic electron temperatures for these sources lie between 2100-5600K. These values of electron temperatures are appreciably less than the temperatures given by RRL studies. In fact all the previous low frequency observations also estimated low electron temperature but because of their low resolutions those results were not regarded as reliable. We have now, with higher resolution data, reaffirmed that electron temperatures are low. This seems to be a generic problem of HII regions and requires further investigation. Further all the diffused extended HII regions in W51A also show higher flux at 240MHz than predicted by thermal spectrum. We propose that each of the above regions comprises of a dense core which is optically thick at frequencies less than about 1GHz. The core is enveloped by a hot ionised medium in the foreground which is optically thin down to 240MHz. Both the components viz., core and envelope, are independent and emit thermally.

5 ACKNOWLEDGEMENTS

PKS acknowledges the support given by IUCAA under its Visiting Associate programme and by NCRA in providing its facilities. PKS also acknowledges the support given by University Grants Commission, India under Project F.8.4(74)/1999-2000/MP.

REFERENCES

Altenhoff W.J., Downes D., Pauls T., Schraml J., 1978, *A&AS*, 35, 23
 Bieging J., 1975, in Wilson T.L., Downes D.H., eds, HII Regions and Related Topics. Springer-Verlag, Berlin, p.443

Churchwell E., Smith L.F., Mathis J., Mezger P.G., Huchtmeier W., 1978, *A&A*, 70, 719
 Copetti M.V.F., Schmidt A.A., 1991, *MNRAS*, 250, 127
 Garay G., Reid M.J., Moran J.M., 1985, *ApJ*, 289, 681
 Goss W.M., Shaver P.A., 1970, *Australian J. Phys. Astrophys. Suppl.*, 14, 1
 Hjellming R.M., Andrews M.H., Sejnowski T.J., 1969, *ApJ*, 157, 573
 Kassim N.E., Weiler K.W., Erickson W.C., Wilson T.L., 1989, *ApJ*, 338, 152
 Kundu M.R., Velusamy T., 1967, *Ann.Astrophys.*, 30, 59
 Martin A.H.M., 1972, *MNRAS*, 157, 31
 Mehringer D.M., 1994, *ApJS*, 91, 713
 Mezger P.G., Henderson A.P., 1967, *ApJ*, 147, 471
 Pankonin V., Payne H.E., Terzian Y., 1979, *A&A*, 75, 365
 Roberts D.A., Goss W.M., 1993, *ApJS*, 86, 133
 Roelfsema P.R., Goss W.M., 1991, *A&AS*, 87, 177
 Shaver P.A., 1969, *MNRAS*, 142, 273
 Shaver P.A., 1980, *A&A*, 91, 279
 Subrahmanyan R., Goss W.M., 1995, *MNRAS*, 275, 755
 van Gorkom J.H., Goss W.M., Shaver P.A., Schwarz U.J., Harten R.H., 1980, *A&A*, 89, 150
 Wilson T.L., Bieging J., Wilson W.E., 1979, *A&A*, 71, 205
 Wilson T.L., Mezger P.G., Gardner F.F., Milne D.K., 1970, *A&A*, 5, 99
 Wood D.O.S., Churchwell E., 1989, *ApJS*, 69, 831